Numerical studies of the combined effects of blast and fragment loading

Ulrika Nyström, Kent Gylltoft

Title: Numerical studies of the combined effects of blast and fragment loading

Authors: Ulrika Nyström, Kent Gylltoft

PII: S0734-743X(09)00052-9
DOI: 10.1016/j.ijimpeng.2009.02.008
Reference: IE 1757

To appear in: *International Journal of Impact Engineering*

Received Date: 22 July 2008
Revised Date: 20 February 2009
Accepted Date: 24 February 2009

Please cite this article as: Nyström U, Gylltoft K. Numerical studies of the combined effects of blast and fragment loading, International Journal of Impact Engineering (2009), doi: 10.1016/j.ijimpeng.2009.02.008

Numerical studies of the combined effects of blast and fragment loading

Ulrika Nyström*, Kent Gylltoft

Department of Civil and Environmental Engineering, Structural Engineering, Concrete Structures, Chalmers University of Technology, SE-412 96 Göteborg, Sweden

(*ulrika.nystrom@chalmers.se)

Abstract

The well-known synergetic effect of blast and fragment loading, observed in numerous experiments, is often pointed out in design manuals for protective structures. However, since this synergetic effect is not well understood it is often not taken into account, or is treated in a very simplified manner in the design process itself. A numerical-simulation tool has been used to further study the combined blast and fragment loading effects on a reinforced concrete wall. Simulations of the response of a wall strip subjected to blast loading, fragment loading, and combined blast and fragment loading were conducted and the results were compared. Most damage caused by the impact of fragments occurred within the first 0.2 ms after fragments' arrival, and in the case of fragment loading (both alone and combined with blast) the number of flexural cracks formed was larger than in the case of blast loading alone. The overall damage of the wall strip subjected to combined loading was more severe than if adding the damages caused by blast and fragment loading treated separately, which also indicates the synergetic effect of the combined loading.

Key-words: Numerical simulation, Blast load, Fragment impact, Combined loading, Concrete

1 Introduction

The combined loading of blast and fragments, caused by explosions, is considered to be synergetic in the sense that the combined loading results in damage greater than the sum of damage caused by the blast

and fragment loading treated separately, [1]. This is a well-known phenomenon pointed out in some of the literature and design manuals within the area of protective design [2]. However, due to the complex nature of the effect of combined loading, its high parameter dependence and the limited number of documentations and comparable experiments, the design manuals often disregard the effect or treat it in a very simplified manner.

In order to increase the understanding of the combined effects of blast and fragment loading, numerical simulations were conducted. The simulations consist of a wall strip subjected to blast and fragment loading, applied both separately and simultaneously. To be able to draw general conclusions about the effect of combined loading the complexities of the structure and the applied loads was reduced. The cases studied in this paper are purely academic, where both the structure and the loads are based on a "real case", i.e. requirements of protective capacity stated in the Swedish Shelter Regulations [3], but are strictly idealized in order to give useful results from which conclusions can be drawn. Using a numerical-simulation tool is motivated by e.g. the high cost of undertaking tests, and the possibility to better follow and understand the principal phenomena related to this kind of loading.

This work is a substudy within a project with the long-term aim to study and increase the knowledge of blast and fragment impacts, and the synergy effect of these loads, on reinforced concrete structures. The research project is a collaboration of many years' duration between Chalmers University of Technology and the Swedish Rescue Services Agency. In earlier studies within the framework of this project, the effect of blast waves in reinforced concrete structures, fragment impacts on plain concrete, and design with regard to explosions and concrete, reinforced and fibre-reinforced, subjected to projectile impact were studied by Johansson [4], Leppänen [5] and Nyström [6,7], respectively.

2 Theoretical framework

2.1 Weapon load characteristics

As detonation of the explosive filler in a cased bomb is initiated, the inside temperature and pressure will increase rapidly and the casing will expand until it breaks up in fragments. The energy remaining after swelling and fragmenting the casing, and imparting velocity to the fragments, expands into the surrounding air and thus creates a blast wave. Thereby, the structures around a bomb detonation will be

exposed to both blast and fragment loading, which means that at least three types of loading effects must be considered:

- impulse load from blast wave
- impulse load from striking fragments
- impact load from striking fragments

where impulse is considered to give a global response and impact a local response caused by the penetration of the fragments.

There are many different types of weapons, designed to have a specific effect on the surroundings. In design of protective structures a threat-determination methodology, based on probability aspects, must be used to decide what load conditions the structure is to be designed for. There are methodologies for calculating the characteristics of the blast and fragment loads caused by explosion, which are well accepted in the design of protective structures. However, even though the blast load characteristics for a bare high-explosive detonation can be estimated with great accuracy, the loads from a cased bomb cannot be determined as accurately [2]. Due to the complexity of not only the blast itself but also the fragmentation of the casing, these load estimations are more uncertain.

Since the properties of the bomb (geometry, casing material and thickness, type of explosive filler, etc.) and its position relative to the target, as well as the surrounding environment, have influence on the loading conditions, all these parameters must be considered during analysis of the loading effect. Also the distance from the detonation (stand-off) will greatly influence the loading properties. This is mainly due to the change in peak pressure for the blast wave and the change in velocity of the fragments, which both decrease with increasing distance. The retardation of the blast wave is larger than that of the fragments, leading to a difference in arrival time. In the range closest to the bomb, i.e. within a few metres, the blast wave will reach the target before the fragments, while at larger distances the fragments will arrive before the blast wave. For a 250 kg general-purpose bomb (GP-bomb), with 50 weight per cent TNT, the blast front and the fragments will strike the target at the same time at an approximate distance of 5 metres; according to Fig. 1, where the time of arrival of the blast load and the fragments are calculated by means of ConWep [8] (based on equations of Kingery and Bulmash [9]) and Janzon [10], respectively.

2.1.1 Blast loading

The blast load resulting from a detonation of an uncased charge in "free air", i.e. distant from the nearest reflecting surface, is well known and often idealised as shown in Fig. 2. The detonation takes place at time $t = 0$ and arrives at the point studied at time t_a. As the blast wave arrives, the pressure increases from the ambient pressure, P_0, to $P_0+P_s^+$, where P_s^+ is the incident overpressure caused by the detonation. As time goes on, the overpressure decays and at time T^+ after the time of arrival the pressure is again equal to the ambient pressure P_0 and the positive phase is over. Due to a partial vacuum formed behind the blast front [11] a negative pressure P_s^- (relative to the ambient pressure) appears and the negative phase is entered. The duration of the negative phase is longer than the positive phase, but the amplitude of the negative pressure is limited by the ambient pressure, P_0, and is often small compared to the peak overpressure, P_s^+. However, in design with regard to explosions the negative phase is considered less important than the positive phase and is therefore often disregarded.

As the blast wave strikes a surface, e.g. a wall, it is reflected and its behaviour changes. The so-called normal reflection, taking place as the blast wave is reflected against a perpendicular surface, may lead to significantly enhanced pressures, where the reflected peak overpressure P_r^+ will be between 2 and 8 [2], and according to [11,12] as much as 20, times higher than the incident overpressure P_s^+. According to [13] the shape of the reflected pressure has the same general shape as the incident pressure, as shown in Fig. 3.

For cased charges the blast load characteristics depend not only on the type and amount of explosive and the stand-off distance, but also on the properties (geometrical and material) of the casing. Since there is less knowledge about how the casing affects the blast wave, there are also less generic expressions describing this. In [14] an expression for calculating an equivalent uncased charge weight is given as a function of the ratio between the casing weight and the actual charge weight. However, the reduced blast pressure due to the energy consumed during casing break-up is often not taken into account in the design manuals [2], which also is used in this study.

2.1.2 Fragment loading

As mentioned earlier, the casing of a bomb will swell after initiation of the explosive filler due to the high pressure. During swelling, cracks will form and propagate in the casing; and as the cracks meet or

reach a free border, fragments are formed [15]. The nose and the tail section of the bomb will break up in a smaller number of massive fragments and the body will fracture into many small fragments.

Derivation of theoretical expressions describing the fragmentation process and its characteristics for cased bombs is difficult. This is partly due to the complexity of the phenomenon itself and partly due to the great variation of bomb properties, which highly influences the fragmentation process. However, there are expressions for estimating the mass distribution and velocities of the fragments that are based on theoretical considerations and confirmed with a large number of tests [16]. In the derivation of these expressions, the bomb casing is normally idealised as a cylinder with evenly distributed explosives, meaning that the methods apply especially to items that can reasonably be approximated as either cylindrical items or as a series of cylindrical items [16]. The more an item deviates from this ideal, the less reliable are the estimations made using these methodologies.

In order to estimate the fragment mass distribution, a relationship developed by Mott [17,18] (presented in e.g. [16,19]) is often used. For design purposes a design fragment is used. The mass of the design fragment is often determined by specifying a confidence level giving the probability that the weight of the fragment is the largest fragment produced. However, this method of determining the design fragment is justified in design where the damage caused by the individual fragments is of interest as the hazardous case. In the case of design against the fragment cluster, another approach may be more desirable where the combined effect of the fragment impact and impulse is of interest. This is discussed further in Section 4.2.

The initial velocity of the fragments can be estimated from the Gurney equation [20] (presented in e.g. [16,19]), which also derives from an assumption of a cylindrical casing. Since this equation is based on energy balance within the explosive and metal case system, without taking into account the loss of energy during rupture of the casing, it is an upper bound estimation.

As the fragments travel through the air their velocity will decrease due to the drag forces. Smaller, lighter fragments will retard faster than larger, heavier fragments. Equations describing this behaviour exist as well, e.g. [16,19].

2.2 Concrete behaviour under static and dynamic loading

It is well known that the two most pronounced disadvantages of concrete are its low tensile strength and brittle behaviour. The tensile strength of normal-strength concrete is less than one tenth of the compressive strength, and after fracture initiation, i.e. after the tensile strength is reached, the ability to transfer stresses through the material decreases rapidly. For high-strength concrete the brittle behaviour can also be seen in the case of uni-axial compression, but the post-fracture ductility in compression increases, with a decreasing compressive strength.

In multi-axial loading conditions the behaviour of concrete differs from the behaviour under uni-axial loading. The ductility, stiffness and strength in compression increase with increased confinement, and for very high lateral pressures the compressive strength may be more than 15 times higher than the uni-axial compressive strength [5]. Such high lateral pressures may occur during impact and perforation of e.g. projectiles and fragments.

High dynamic loading, giving a high strain rate in the material, also affects the strength and ductility of the concrete. In the case of high-rate tensile loading, the ultimate uni-axial tensile strength may be as much as 5 to 7 times higher than the static tensile strength [21], and even though the effect on the ultimate compressive strength is less pronounced it may still be more than doubled [22]. It has recently also been indicated that the fracture energy is strain-rate-dependent [23-25].

3 Method

Tests have been conducted around the world to study the combined effects of blast and fragment loading, but these are often not suitable for drawing general conclusions about the local or global structural behaviour. This is due to the great variation of parameters involved, e.g. load characteristics and stand-off, which affects the results. Numerical simulations are often used to investigate the effect of blast and fragments, and make it possible to study the influence of different parameters – stand-off distance, fragment size, materials etc. – which is costly in experimental testing. Nevertheless, the numerical simulations cannot fully supersede experiments, but should be used in combination, and experiments are needed to verify the numerical models used in the simulations.

The reinforced concrete structure used in the study presented here are based on a wall strip in a civil defence shelter, fulfilling the requirements of protective capacity related to conventional bombs in the Swedish Shelter Regulations [3]. The loads applied, i.e. the blast wave and fragment loading, are also based on the load definitions in [3].

As no suitable experiments, with combined blast and fragment loading, were found for this study, two separate experiments on blast load and single fragment impact were used to verify and calibrate the numerical model. The validation and calibration process was done within a preliminary study and is only briefly described in this paper. Conclusions from the preliminary study were used to build up the numerical model of the wall strip subjected to blast and fragment impacts used in the main study. Single-degree-of-freedom analyses were used to find what load combination caused the largest deflection: simultaneous arrival of the two loads, blast load arriving first, or fragments arriving first. The results from the SDOF analyses were used to decide the arrival times for the loads in the numerical simulation of combined loading. The numerical results of the wall-strip response were compared and analysed in order to see the effects of combined loading.

For further information about this study the reader is referred to [26] where a detailed description of the load characterisation and the preliminary study is presented.

4 Wall element and load characteristics

The Swedish Shelter Regulations [3] govern the design of civil defence shelters in Sweden, and contain the requirements specified for these protective structures. Here only the criteria for protective capacity related to conventional bombs are specified, but it should be pointed out that civil defence shelters also are designed to withstand e.g. radioactive radiation, chemical and biological warfare, and explosive gases.

According to [3], a civil defence shelter should be designed to withstand the effect of a pressure wave corresponding to that produced by a 250 kg GP-bomb with 50 weight per cent TNT, which bursts freely outside at a distance of 5.0 metres from the shelter during free pressure release. Further, the shelter must also be able to withstand the effect of fragments from a burst as described above. In the case of fragment

loading it is the fragment cluster that is meant, while larger individual fragments may damage and penetrate the shelter.

4.1 Wall element

In the Swedish Shelter Regulations [3], the civil defence shelter is conceived as a reinforced, solid concrete structure. For a shelter without backfilling the minimum thicknesses of the roof, walls and floor are specified as 350, 350 and 200 mm, respectively, and the concrete should fulfil a requirement of at least C25/30, according to [27] (corresponds to mean cylindrical compressive strength of 25 MPa). Hot-rolled reinforcement bars with a specified requirement of strain hardening must be used. The reinforcement must be placed in two perpendicular alignments in both edges of the structural element and the minimum and maximum reinforcement content is 0.14 and 1.10%, respectively. A minimum reinforcement-bar diameter of 10 mm and maximum bar spacing of 200 mm are required, with a maximum concrete cover of 50 mm.

The wall studied has a total height of 3 metres and is simplified to be simply supported with a span length of 2.7 m, as seen in Fig. 4. The rough simplification of the support conditions was not made in an attempt to imitate the real behaviour of the wall.

In [3], equivalent static loads, representing the weapon effect, are used in the design process. A static load of 50 kN/m^2 is used to calculate the required amount of reinforcement in the walls, giving reinforcement bars ø10 s170 (465 mm^2/m in each face of the wall element). Deformed reinforcement bars (B500BT), with a yield strength of 500 MPa were assumed and the distance from concrete edge to centre of reinforcement bars was chosen as 35 mm. The concrete was assumed to have a concrete strength of 35 MPa.

4.2 Load characteristics

In Fig. 5 the blast load caused by the GP-bomb specified in Section 4 with a stand-off of 5.0 metres, calculated with ConWep [8], is shown together with a simplified relationship. It should be kept in mind that design codes do often not take into account the energy consumed for swelling and fragmenting the

casing of bombs. As an approximation this energy loss is also neglected in the present study even though it would be more accurate to reduce the pressure of the blast load in order to imitate the real behaviour. The blast load is assumed to be uniform over the wall, which is reasonably accurate for this stand-off [4]. The impulse density of the blast load is, according to [8], 2 795 Ns/m^2.

Since the geometry and casing material of the bomb used in the design of civil defence shelters are not specified, the size and mass distribution cannot be calculated without making certain assumptions. In this study, the American GP-bomb Mk82 was used as a reference when estimating the mass distribution of the bomb specified in the Swedish Shelter Regulations. According to ConWep [8] the Mk82 has a nominal weight of 500 lb (226.8 kg) and contains 192.0 lb (87.09 kg) of the high explosive H-6, corresponding to 242.9 lb (110.2 kg) equivalent weight of TNT, and is therefore relatively close to the bomb specified in the Swedish Shelter Regulations [3]. The mass distribution was estimated by scaling the inner casing diameter and the casing thickness to correspond to the somewhat increased volume of explosive filler compared to the Mk82; for more details see [26].

All fragments used in the simulations were assumed to be spherical and of the same size, corresponding to a design fragment. It was further assumed that the fragments were uniformly distributed over the wall. Even though these idealizations are rough and differ from the real fragment loading caused by a bomb, where the mass, shape and velocity of the fragments differs and the distribution of the fragments over the wall is not uniform, they were necessary in order to reduce the complexity of both the numerical model and the results produced. It can be pointed out that a more realistic fragment mass distribution would give a more non-uniform damage over the wall, where the larger fragments would give a larger local damage than the smaller fragments.

As mentioned in Section 2.1.2, the design fragment, calculated with a confidence level (often taken as 95%), is used for design with regard to fragment impact. However, this design fragment and the corresponding effect on the target are not representative of the fragment impulse load which is important to capture the global response caused by the fragments and not only their local effect. This means that another approach must be used to find a representative fragment size in this study and it was decided to use the impulse caused by the real fragment load on the wall, caused by a vertically placed bomb, to define a representative weight of the fragments. From estimations of the mass and velocity distribution among the fragments, the corresponding fragment impulse distribution was calculated, and a

representative fragment size was determined as the fragment mass giving the average impulse on the structure, for details see [26]. This resulted in a fragment mass of 21.9 g and a fragment diameter of 17.5 mm. The initial fragment velocity was calculated to approximately 1 890 m/s (by use of the Gurney equation), and at the distance of 5.0 metres the velocity is decreased to 1 760 m/s. The fragment density is approximately 0.65 kg/m^2 and the corresponding impulse intensity caused by the fragments is 1 125 Ns/m^2.

4.3 SDOF estimations

The single-degree-of-freedom method (SDOF method) was used in order to find what combination of arrival times of the blast and fragment load that resulted in the maximum deflection. The simplified relation of the blast load, presented in Section 4.2, was used for the blast load and a triangular load was assumed for the fragment loading. The duration of the fragment loading was assumed to 0.1 ms, which is the approximate time it takes for the fragment to penetrate the concrete, and its impulse intensity was as defined in Section 4.2, giving a peak pressure of 22.5 MPa. It should be pointed out that only the impulse load of the fragments was taken into consideration in the SDOF analyses presented in this paper, since the penetration by the fragments and the subsequent damage were not considered. An ideal-plastic material response of the SDOF system was used and the maximum value of the internal dynamic resistance R_m of the wall strip was calculated to be 275 kN; for details see Appendix A and [26].

In Fig. 6 the results are shown for five different cases of combined loading:

1. loads arrive at the same time (simultaneous loading)
2. blast wave first, fragments arrive at maximum wall velocity caused by the blast
3. blast wave first, fragments arrive at maximum wall deflection caused by the blast
4. fragments first, blast wave arrives at maximum wall velocity caused by the fragments
5. fragments first, blast wave arrives at maximum wall deflection caused by the fragments

As seen, the case of simultaneous loading causes the most severe deflection (equalling 139.2 mm at time 42.2 ms). For further information about the SDOF method the reader is referred to [6] and [19].

5 Numerical model

Hydrocodes are used for highly time-dependent dynamic problem-solving by use of finite difference, finite volume and finite element techniques. The differential equations for conservation of mass, momentum and energy, together with material models, describing the behaviour of the materials involved, and a set of boundary conditions give the solution of the problem. The numerical hydrocode AUTODYN 2D and 3D [28] was used in this study, and the Lagrangian solver technique was employed.

5.1 Calibration and validation of numerical model

Experiments and findings from numerical simulations of experiments described in the literature were used in the calibration and validation process for the numerical model used in this study. The numerical simulations for the calibration process were performed in 2D and 3D. The use of 2D was to prefer since it reduces the computational time, but since beam elements (used to simulate the reinforcing bars) could not be used in the 2D simulations, 3D was used when reinforced concrete were simulated. However, 3D was used with the width of one element and use of boundary conditions to emulate a 2D simulation. Below is a brief summary of the calibration and validation process; for further description see [26].

Magnusson and Hansson [29] described experiments on reinforced concrete beams, of length 1.72 m, subjected to blast loading, and thereafter used AUTODYN 3D to simulate the beam response. They concluded that it was possible to simulate the beam response with the RHT material model provided that the principal-stress tensile-failure model with a fully associated flow rule (i.e. the flow rule was associated in both the deviatoric and meridian planes) was used in the simulations, together with crack softening. This was also found by means of numerical simulations of the same experiment conducted within the calibration process made in the study presented here. In this process it was also found that an element length of 12 mm gave approximately the same beam response as a finer mesh of 6-mm elements; hence, the coarser mesh of 12-mm elements should be accurate enough to simulate the beam response when subjected to blast loading.

Leppänen [30] performed and described experiments with a single fragment impacting a concrete block, with size 750 x 350 x 500 mm. An AUTODYN 2D model with axial symmetry and different element sizes (1 and 2 mm) was used in the calibration process, and it was concluded that the numerical

model gave accurate results. However, the size of the fragment used in [30] differed from the fragment size used in this study, and hence, additional 2D simulations were conducted to investigate the effect of the element size. It was concluded that the resulting crater in the simulations with an element size of 6 mm was somewhat different from the crater in simulations where smaller elements were used, but still an acceptable approximation of the damage caused by the fragment impact. Thus, it was not considered worth the greatly increased computational time to use a finer mesh in the main study.

5.2 Material models

The standard material model for concrete with compressive strength of 35 MPa in the material library of AUTODYN was used to describe the behaviour of concrete. This material model was developed by Riedel, Hiermayer and Thoma (therefore called the RHT model) [31], and consists of three pressure-dependent surfaces in the stress space. The RHT model also takes into account pressure hardening, strain hardening and strain-rate hardening as well as the third invariance in the deviatoric plane. However, the preliminary study, i.e. the calibration and validation process described in Section 5.1, showed that it was necessary to make some modifications within the model to get accurate results. For example, it was concluded that a principal-stress tensile-failure model was necessary to describe the behaviour of the wall strip in the case of blast loading, instead of the hydrodynamic tensile-failure model used as default in the RHT model. The change to a principal-stress tensile-failure model leads to a cut-off of the strain-rate dependence of the ultimate tensile strength.

To describe the behaviour of the reinforcing steel, a piecewise linear Johnson-Cook material model was used, including strain hardening but not strain-rate and thermal effects. A linear elastic steel material model, with a shear modulus of 81.1 GPa, was used for the supports, and a von Mises material model, simplifying the material behaviour to linear-elastic–ideal-plastic with yield strength of 800 MPa, was used for the fragments. A linear equation of state (*EOS*) was used for the reinforcing steel, the supports and the fragments, while the nonlinear *P-α EOS* was used for the concrete. The input in the different material models used in the simulations are presented in Tables 1 to 3; for further information about the material models used, the reader is referred to [26,31,32].

5.3 Mesh

Since fragment penetration is a local effect, requiring relatively small elements, a numerical model of even a 1.0-metre wide strip of the shelter wall would have been very large and required extensive computational time. By use of symmetries and plane-strain-boundary conditions the model was limited to a 84 x 1 512 x 350 mm part of the wall, representing 4.25% of a metre-wide wall strip which reduces the total number of elements used in the model from approximately 2.3 million to 98 106. Even though the width of the wall strip is only 9.6 times the fragment dimension and the size of the front face crater caused by the fragment impact (measured in the 2D simulations used for calibration described in Section 5.1) approximates the width of the wall strip included in the model the use of plane-strain-boundary conditions are applicable. The plane-strain-boundary condition takes into account the next row of fragments which strikes the wall 168 mm from the row of fragments included in the model. Including a wider part of the wall in the model, where the choice of width of course has to be done with respect to the loading case, would only lead to negligible changes in the results.

Due to the varying need of element sizes when simulating the effects of blast and fragment impact, a finer mesh of Lagrangian elements (size 6 x 6 x 6 mm) was used on the front face of the wall strip, and a coarser mesh of elements (size 12 x 12 x 6 mm) of the same element type was used on the rear side of the wall strip (see Fig. 7), resulting in a total number of 97 020 concrete elements, where 59 976 of those were in the front zone where the finer mesh was used and 37 044 in the rear zone with the coarser mesh. The total number of elements along the depth (x-direction), the height (y-direction) in the front- and rear-zones, and the width (z-direction) of the concrete structure included in the model were, 38, 252, 126 and 14, respectively.

The wall strip was supported by two semicylindrical supports with a radius of 84 mm to avoid local crushing of the elements around the supports. The nodes of the support were joined together with the interfacing concrete nodes. In order to allow for rotation around the supports only the line of back nodes was prevented from moving in the x-direction. The supports were modelled with 4 elements along the radius of the half-cylinders, resulting in a total number of 336 elements in one support.

In the simulations including impacting fragments, these were modelled with two elements along their radius, resulting in 16 elements per half-fragment and a total number of 120 fragment elements in the model. Embedded beam elements with the same length as the surrounding concrete elements and with

circular cross-section were used to model the reinforcement bars, giving a total number of 630 beam elements in the model.

6 Results

The responses of the wall strip estimated in the numerical simulations for blast loading, fragment loading, and combined blast and fragment loading (simultaneous loading) are presented and discussed below. As the damage differs at different locations within the wall strip, the damage is shown in three views for each case: a top view, a side view at the section of reinforcement, and one in the middle of the wall strip (the section where the fragments strike the wall strip). In the figures with the wall strip responses, the colour red indicates fully damaged concrete.

6.1 Blast loading

In the case of blast loading, the maximum deflection is 65.2 mm and takes place 29.0 ms after the arrival. In Fig. 8 the damage in the wall strip is shown at time of maximum deflection, where it can be seen that cracks have formed at the rear side of the wall strip and have propagated towards the front face. The damage is localised to relatively few cracks, even though it can be seen that crack initiation has taken place rather densely along the length of the strip. Damaged concrete can also be seen along the reinforcement close to the fully developed cracks; at these locations the reinforcement bars were yielding.

When studying the crack development, it was seen that the localised crack closest to the support was formed already after 1 ms, while no damage of the concrete was observed in the middle of the beam at this time. This indicates a direct shear crack due to the inertia effects, i.e. internal momentum, related to severe dynamic loading. After approximately 2 ms, also the localised cracks in the middle of the beam have formed, and these have the character of flexural cracks.

6.2 Fragment loading

In Fig. 9 the wall strip subjected to fragment loading is shown at time of maximum deflection. This is reached 13.3 ms after the fragments strike the wall, and amounts to 11.0 mm. As can be seen, the simulated damage caused by the multi-fragment impact is more complex than in the case of blast loading. The total damage consists of local damage on the front face, i.e. craters, scabbing cracks at the rear of the wall strip, direct shear cracks close to the supports, and bending cracks in the more central parts of the beam. When comparing Fig. 8 and Fig. 9, it can be seen that there are more bending cracks formed in the case of fragment impact than for blast loading, resulting in an increased energy-absorbing capacity since the reinforcement bars can yield at more locations. This means that also the load-bearing capacity may increase. However, the load-bearing capacity will at the same time be reduced by the decreased effective height due to the damage on the front face of the wall strip.

To better distinguish the modes of damage and to better understand their evolution, the beam response is shown at different times, i.e. after 0.25, 0.6 and 9 ms, in Fig. 10. After 0.25 ms (Fig. 10a) the fragment impacts have caused craters on the front face, and the reflected stress wave has caused scabbing cracks at the rear of the wall strip. The scabbing effect was not expected in the simulations, but 2D simulations of fragment impact, taking the multiple simultaneous impact of fragments and also the strain-rate dependence of the tensile strength into account, confirm this behaviour; see [26]. However, in reality the two scabbing cracks probably represent one crack which appears at the level of tensile reinforcement and not in between the two reinforcement layers, as in this case.

Approximately 0.6 ms after the arrival of fragments, cracks propagate at the rear side of the wall strip, close to the supports, see Fig. 10b. These are probably direct shear cracks, as also observed in blast loading; see Section 6.1.

At time 9 ms, flexural cracks have started to propagate in the wall strip, as seen in Fig. 10c. These cracks form at the rear face of the target, but also at the level of the scabbing cracks, which indicates that the wall strip has started to act as two separate structures with sliding between the two separate planes formed by the horizontal scabbing cracks.

6.3 Combination of blast and fragment loading

The maximum mid-point deflection in case of simultaneous loading of blast and fragment is 85.7 mm and occurs after 33.4 ms. The response of the wall strip at time of maximum deflection is shown in Fig. 11. As the damage caused by the fragment impact, i.e. the front face craters and the scabbing cracks at the rear of the strip, appears very early (at less than 0.25 ms, as seen in Section 6.2) the damage in the case of combined, simultaneous loading is rather similar to the case of fragment loading alone. Due to the blast load, the deflection is larger and the damage in the concrete surrounding the reinforcement bars is more severe than in the case of fragment impact alone.

Further, the diameters of the front face craters are reduced in case of combined loading compared to fragment loading alone. This can probably be explained by increased confinement effects. The blast wave causes pressure on the front face, acting perpendicular to the concrete surface, and gives a lateral pressure to the material compressed by the fragment penetration; schematically shown in Fig. 12. This reduction of front-face damage may lead to a higher load-bearing capacity than in the case with fragment impacts alone, but since the effective height of the wall strip is reduced, the load-bearing capacity is still affected. However, as in the case of fragment loading alone, the number of flexural cracks formed is larger than in the case of blast loading alone, allowing the reinforcement bars to yield at more locations, which may improve the load-bearing capacity.

7 Comparison of mid-point deflections and velocities

In Fig. 13 the mid-point deflections of the three wall strips subjected to blast, fragment and combined loading, respectively, are shown. As seen, the mid-point deflection in the case of combined loading is larger than the sum of the deflections caused by blast and fragment loading separately, which indicates a synergy effect.

In Fig. 14 the mid-point velocities from the simulations with blast, fragment and combined loading are shown. The velocity for combined loading is first influenced by the fragment impact, but already after a fraction of a millisecond the velocity seems close to the velocity of the wall strip subjected to blast loading alone. After approximately 2 ms, the velocity for combined loading increases and exceeds the velocity for blast loading.

In Table 4 the mid-point deflections estimated in the numerical analyses are presented together with results from SDOF analyses. Input parameters for the SDOF analyses are shown in Appendix A.
In the case of blast loading the estimations of the deflection made in SDOF and numerical simulations agree well. In the case of fragment loading the difference is larger, which probably can be explained by the limitations in the SDOF analyses to take into account e.g. the energy consumed during penetration and subsequent crushing of the concrete, the formation of many flexural cracks, and inertia effects, which may increase the load-bearing capacity. The results from the numerical simulation and the SDOF analysis differ also for combined loading. The difference is even larger than in the case of fragment loading and ay be explained by magnification of the limitations already used as explanation for the case of fragment loading.

8 Summary and conclusions

In blast loading, the elongation of the rear face of the wall strip is localised to a few cracks where yielding of the reinforcement takes place. In fragment loading, the flexural cracks to which the elongation of the reinforcement is localised are numerous, the energy-absorbing capacity of the wall strip may thus be increased.

In the simulations involving fragment loading, scabbing cracks formed due to the reflected stress wave. The appearance of these cracks were unexpected, but was confirmed with a 2D simulation study, indicating that the case of multi-fragment impact may lead to scabbing also when the single fragment impact does not. It may therefore be necessary to take this effect into account in design of protective structures. However, it is questionable whether the location and size of the scabbing cracks simulated are realistic.

Most damage caused by the fragment impact occurs within 0.2 ms after arrival, which is short compared to the response time of the element, indicating that in the case of combined loading the bearing capacity and the mid-point deflection of the wall strip may be highly influenced by the fragment impact since the structure thus loses part of its effective height.

The larger mid-point deflection of the wall strip subjected to blast loading, compared to the deflection in the case of fragment loading, was expected since the impulse from the blast was almost 2.5 times the impulse caused by the fragments.

The damage caused by combined loading is more severe than if adding the damages caused by the blast and fragment loading treated separately. The size of the front face craters, though, is an exception since these are larger in the case of fragment loading than in combined loading. It can be concluded that the mid-point deflection in combined loading (85.7 mm) is larger than the sum of mid-point deflections for blast and fragment loading treated separately (in total 76.2 mm), indicating a synergy effect in combined loading.

Acknowledgement

The work presented in this paper is done within the research project "Concrete structures subjected to blast and fragment impacts: dynamic behaviour of reinforced concrete", financially supported by the Swedish Rescue Services Agency. The authors would like to thank the members of the reference group for the project: Björn Ekengren, M.Sc., at the Swedish Rescue Services Agency, Morgan Johansson, Ph.D., at Reinertsen AB, and Joosef Leppänen, Ph.D., at FB Engineering AB.

References

[1] Girhammar UA. Brief review of Combined Blast and Fragment Loading Effects. Report C7:90. National Fortifications Administration, Eskilstuna, Sweden, 1990. 15 pp.

[2] ASCE. *Structural Design for Physical Security – State of the Practice*. Task committee: Conrath, E.J. *et al*., American Society of Civil Engineers, 1999. 264 pp.

[3] Ekengren B. Skyddsrum SR 06 (Shelter regulations SR06, in Swedish). Swedish Rescue Services Agency, Karlstad (Sweden), 2006. 113 pp.

[4] Johansson M. Structural Behaviour in Concrete Frame Corners of Civil Defence Shelters, Non-linear Finite Element Analyses and Experiments. Doctoral Thesis, Department of Structural Engineering, Concrete Structures, Göteborg (Sweden): Chalmers University of Technology, 2000. 220 pp.

[5] Leppänen J. Concrete Structures Subjected to Fragment Impacts, Dynamic Behaviour and Material Modelling. Doctoral Thesis, Department of Structural Engineering and Mechanics, Concrete Structures, Göteborg (Sweden): Chalmers University of Technology, 2004. 127 pp.

[6] Nyström U. Design with regard to explosions. Master's Thesis, Department of Civil and Environmental Engineering, Structural Engineering, Concrete Structures, Göteborg (Sweden): Chalmers University of Technology, 2006. 205 pp.

[7] Nyström U, Leppänen J. Numerical Studies of Projectile Impacts on Reinforced Concrete. In: Fan C, Chua HK (eds.). Proceedings of the Second International Conference on Design and Analysis of Protective Structures, Singapore (Singapore): Nanyang Technical University, 2006. p. 310-319.

[8] ConWep. Collection of conventional weapon effects calculations based on TM 5-855-1, Fundamentals of Protective Design for Conventional Weapons, U. S. Army Engineer Waterboys Experiment Station, Vicksburg (VA, USA), 1992.

[9] Kingery CN, Bulmash G. Air Blast Parameters from TNT Spherical Air Burst and Hemispherical Surface Burst. US Army Ballistic Research Laboratory Technical Report ARBRL-TR 02555, Aberdeen Providing Ground, MD, 1984.

[10] Janzon B. Grundläggande Stridsdelsfysik (in Swedish). National Defence Research Establishment (FOA), FOA report C 20261-D4, Stockholm (Sweden), 1978. 168 pp.

[11] Johansson M, Laine L. Bebyggelsens motståndsförmåga mot extrem dynamisk belastning, Delrapport1: Last av luftstötvåg (The capacity of buildings to resist severe dynamic loading, Part 1: Blast wave loading, in Swedish). Swedish Rescue Services Agency, Karlstad (Sweden) 2007. 114 pp.

[12] Baker WE. Explosions in Air. University of Texas Press, Austin (TX, US), 1973. 285 pp.

[13] U.S. Army. Fundamentals of Protective Design for Conventional Weapons. Technical Manual TM 5-855-1. 1992. 271 pp.

[14] Forsén R, Nordström M. Damage to reinforced concrete slabs due to the combination of blast and fragment loading. (Reprint from the Second International Conference of Structures under Shock and Impact, Portsmouth, UK, 1992.) FOA report B 20101-2.6. National Defence Research Establishment, Sundbyberg (Sweden), 1992. 12 pp.

[15] Curran DR. Simple fragment size and shape distribution formulae for explosively fragmenting munitions. Int J Impact Engng 1997;20:197-208.

[16] DDESP. Methodologies for calculating primary fragment characteristics. Report No. DDESP TP 16, Department of Defence Explosives Safety Board, Alexandra, (U.S.), 2003. 53 pp.

[17] Mott NF, Linfoot EH. A Theory of Fragmentation. Ministry of Supply report No A.C.3348, January 1943.

[18] Mott NF. A Theory of Fragmentation of Shells and Bombs. Ministry of Supply report No A.C.4035, May 1943.

[19] Krauthammer T. Modern protective structures – Design, analysis and evaluation. Course notes for course Modern Protective Structures, State College (USA), July 2006. 412 pp.

[20] Gurney RW. The Initial Velocities of Fragments from Bombs, Shells and Grenades. US Army Ballistic Research Laboratory Report BRL 405, Aberdeen Providing Ground, MD, September 1943.

[21] Malvar LJ, Ross CA. Review of Strain Rate Effects for Concrete in Tension. ACI Mater J 1998;95(6):735-739.

[22] Bischoff PH, Perry SH. Compressive behaviour of concrete at high strain rates. Mater Struct 1991;24:425-450.

[23] Schuler H. Experimentelle und numerische Untersuchungen zur Schädigung von stoßbeanspruchtem Beton (in German). Doctoral Thesis, Universität der Bundeswehr München, Freiburg (Germany): Institut Kurzzeitdynamik, Ernst-Mach-Institut, 2004. 184 pp.

[24] Brara A, Klepaczko JR. Fracture energy of concrete at high loading rates in tension. Int J Impact Engng 2007;34(3):424-435.

[25] Weerheijm J, van Doormaal JCAM. Tensile failure of concrete at high loading rates: New test data on strength and fracture energy from instrumented spalling tests. Int J Impact Engng 2007;34(3):609-626.

[26] Nyström U. Concrete Structures Subjected to Blast and Fragment Impacts, Numerical Simulations of Reinforced and Fibre-reinforced Concrete. Licentiate thesis. Department of Civil and Environmental Engineering, Structural Engineering, Concrete Structures, Göteborg (Sweden): Chalmers University of Technology, 2008. 117 pp.

[27] Boverket. Boverkets Handbok för Betongkonstruktioner BBK 04, (Boverket's handbook for Concrete Structures BBK 04, in Swedish). Boverket, Karlskrona (Sweden), 2004. 271 pp.

[28] ANSYS AUTODYN User Manual, Version 11.0. Concord (CA, USA): Century Dynamics Inc., 2007. 528 pp.

[29] Magnusson J, Hansson H. Simuleringar av explosionsbelastade betongbalkar – en principstudie (Numerical simulations of concrete beams – a principal study, in Swedish). National Defence Research Establishment (FOI), FOI Report 1686--SE, Tumba (Sweden), 2005. 55 pp.

[30] Leppänen J. Splitterbelastad betong – Experiment och numeriska analyser (Fragment Impacts into Concrete – Experiments and Numerical Analyses, in Swedish). Department of Structural Engineering and Mechanics, Division of Concrete Structures, Chalmers University of Technology, Report no. 03:6, Göteborg (Sweden), 80 pp.

[31] Riedel W. Beton unter dynamischen lasten, meso. und makromechanische modelle und ihre parameter (in German). Doctoral Thesis, Universität der Bundeswehr München, Freiburg (Germany): Institut Kurzzeitdynamik, Ernst-Mach-Institut, 2000. 210 pp.

[32] AUTODYN Theory Manual, Revision 4.3. Concord (CA, USA), Century Dynamics Inc., 2005. 227 pp.

[33] Magnusson J, Hallgren M. High Performance Concrete Beams Subjected to shock Waves from Air Blast. National Defence Research Establishment (FOA), FOA report 00-01586-311--SE, Tumba (Sweden), 2000. 86 pp.

[34] Johansson M. Stötvågsutbreding i luft (Blast wave in air, in Swedish). Swedish Rescue Services Agency, Karlstad (Sweden), 2002. 60 pp.

Appendix A

Since an ideal-plastic material behaviour was assumed for the internal resistance of the SDOF system the equation of motion used to describe the movement of the mid-point in a simply supported beam, with mass, M, and length, L, subjected to a uniformly distributed load, $q(t)$, can be simplified to:

$$\frac{2}{3} M \ddot{u} + R = q(t) \cdot L \qquad (1)$$

where $\ddot{u}$ is the mid-point acceleration of the beam [6].

When assuming an ideal-plastic material behaviour, the internal resistance, R, in Eq. 1 equals the maximum value of the load that the beam (or wall strip) can bear, i.e. $R=R_m$ given that the displacement $u\neq0$. Before any displacement occurs ($u=0$), if the external load is smaller than the maximum load-

bearing capacity ($P(t)<R_m$), the internal resistance equals the external load ($R=P(t)$). According to [13] the dynamic internal resistance can be estimated as 1.3 times the static internal resistance, possible explanation to this is given in [26]. The increase in load-bearing capacity in the case of dynamic loading, compared to static loading, is reported in [33] where blast-loaded concrete beams are studied, and supports the value used in [13] for increased internal resistance to dynamic loads. In numerical simulations of blast-loaded walls conducted and reported by Johansson [34] an increased load-bearing capacity was observed. [34] explained this by the appearance of large normal forces, which probably can be explained by inertia effects.

The dynamic internal resistance, R_m, is for a simply supported beam with uniformly distributed load thus calculated as:

$$R_m = 1.3 \frac{8 M_{Rd}}{L} \tag{2}$$

where M_{Rd} is the static moment capacity of the beam.

Fig. 1. Time of arrival for blast wave and fragments as functions of the stand-off for a 250 kg GP-bomb with 50 weight per cent TNT, from [5].

Fig. 2. Incident blast wave idealisation for 125 kg TNT at 5 meters stand-off, based on [4].

Fig. 3. Positive phase of reflected and incident blast wave for 125 kg TNT at 5 metres stand-off, calculated according to [13].

Fig. 4. Civil defence shelter and simplified model of one of its walls.

Fig. 5. The reflected pressure load as function of time for 125 kg TNT at a distance of 5.0 metres, according to ConWep [8], and the simplified relationship for this which is used in this study, based on [4].

Fig. 6. Mid-point deflection of wall strip subjected to blast load and fragment impulse load, calculated with SDOF method. Since the response of simultaneous loading and loading where fragments arrive first and blast at time of maximum velocity are almost identical these lines are seen as one in the figure.

Fig. 7. Numerical mesh of wall strip used in simulations, also showing reinforcement in the modelled wall strip.

Fig. 8. Response of wall strip subjected to blast load at time of maximum mid-point deflection.

Fig. 9. Response of wall strip subjected to fragment impacts at time of maximum mid-point deflection.

Fig. 10. Response of wall strip subjected to fragment impacts at time (a) 0.25 ms, (b) 0.6 ms and (c) 9 ms after time of fragment arrival, seen at section of reinforcement.

Fig. 11. Response of wall strip subjected to combined blast and fragment loading at time of maximum mid-point deflection.

Fig. 12. Schematically shown confinement effects from blast loading, σ_{blast}, on concrete element compressed by $\sigma_{fragment}$ due to fragment penetration.

Fig. 13. Mid-point deflection of wall strip subjected to combined, blast and fragment loading from numerical simulations.

Fig. 14. Mid-point velocity of wall strip subjected to blast and fragment loading from numerical simulations.

Table 1.

Employed material data for concrete, input to the RHT model.

Table 2.

Employed material data for reinforcing steel.

Table 3.

Employed material data for supports and fragments.

Table 4.

Mid-point deflections.

Equation of state	**P alpha**	Brittle to ductile transition	1.05000E-02 (-)
Reference density	2.75000E+00 (g/cm^3)	G (elastic)/(elastic-plastic)	2.00000E+00 (-)
Porous density	2.31400E+00 (g/cm^3)	Elastic strength/f_t	7.00000E-01 (-)
Porous soundspeed	2.92000E+03 (m/s)	Elastic strength/f_c	5.30000E-01 (-)
Initial compaction pressure	2.33000E+04 (kPa)	Fractured strength constant B	1.60000E+00 (-)
Solid compaction pressure	6.00000E+06 (kPa)	Fractured strength exponent M	6.10000E-01 (-)
Compaction exponent	3.00000E+00 (-)	Compressive strain rate exponent α	3.20000E-02 (-)
Solid *EOS*	Polynomial	Tensile strain rate exponent δ	3.60000E-02 (-)
Bulk modulus *A1*	3.52700E+07 (kPa)	Max. fracture strength ratio	1.00000E+20 (-)
Parameter *A2*	3.95800E+07 (kPa)	Use *CAP* on elastic surface?	Yes
Parameter *A3*	9.04000E+06 (kPa)	**Failure**	**RHT concrete**
Parameter *B0*	1.22000E+00 (-)	Damage constant *D1*	4.00000E-02 (-)
Parameter *B1*	1.22000E+00 (-)	Damage constant *D2*	1.00000E+00 (-)
Parameter *T1*	3.52700E+07 (kPa)	Minimum strain to failure	1.00000E-02 (-)
Parameter *T2*	0.00000E+00 (kPa)	Residual shear modulus fraction	1.30000E-01 (-)
Reference temperature	3.00000E+02 (K)	Tensile failure	Principal stress
Specific heat	6.54000E+02 (J/kgK)	Principal tensile failure stress	3.50000E+03 (kPa)
Compaction curve	Standard	Max. principal stress difference/2	1.01000E+20 (kPa)
Strength	**RHT concrete**	Crack softening	Yes
Shear modulus	1.67000E+07 (kPa)	Fracture energy, G_F	1.20000E+02 (J/m^2)
Compressive strength (f_c)	3.50000E+04 (kPa)	Flow rule	Bulking (Associative)
Tensile strength (f_t/f_c)	1.00000E-01 (-)	Stochastic failure	No
Shear strength (f_s/f_c)	1.80000E-01 (-)	**Erosion**	**Geometric strain**
Intact failure surface constant A	1.60000E+00 (-)	Erosion strain	2.00000E+00 (-)
Intact failure surface exponent N	6.10000E-01 (-)	Type of geometric strain	Instantanous
Tens./Comp. meridian ratio (Q)	6.80500E-01 (-)		

Equation of state	**Linear**	Eff. Plastic strain #10	1.00000E+01 (-)
Reference density	7.83000E+00 (g/cm^3)	Yield stress #1	5.62000E+05 (kPa)
Bulk modulus	1.59000E+08 (kPa)	Yield stress #2	5.68000E+05 (kPa)
Reference temperature	3.00000E+02 (K)	Yield stress #3	6.27000E+05 (kPa)
Specific heat	4.77000E+00 (J/kgK)	Yield stress #4	6.78000E+05 (kPa)
Thermal conductivity	0.00000E+00 (J/mKs)	Yield stress #5	7.15000E+05 (kPa)
Strength	**Piecewise JC**	Yield stress #6	7.46000E+05 (kPa)
Shear modulus	8.18000E+07 (kPa)	Yield stress #7	7.76000E+05 (kPa)
Yield stress (zero plastic strain)	5.49330E+05 (kPa)	Yield stress #8	7.95000E+05 (kPa)
Eff. Plastic strain #1	6.70000E-03 (-)	Yield stress #9	7.95000E+05 (kPa)
Eff. Plastic strain #2	1.62000E-02 (-)	Yield stress #10	7.95000E+05 (kPa)
Eff. Plastic strain #3	2.86000E-02 (-)	Strain rate constant *C*	0.00000E+00 (-)
Eff. Plastic strain #4	4.57000E-02 (-)	Thermal softening exponent *m*	0.00000E+00 (-)
Eff. Plastic strain #5	6.45000E-02 (-)	Melting temperature	0.00000E+00 (K)
Eff. Plastic strain #6	9.21000E-02 (-)	Ref. strain rate (1/s)	1.00000E+00 (-)
Eff. Plastic strain #7	1.27800E-01 (-)	**Failure**	**None**
Eff. Plastic strain #8	1.79200E-01 (-)	**Erosion**	**None**
Eff. Plastic strain #9	1.79201E-01 (-)		

Equation of state	**Linear**	**Equation of state**	**Linear**
Reference density	7.83000E+00 (g/cm^3)	Reference density	7.83000E+00 (g/cm^3)
Bulk modulus	1.59000E+08 (kPa)	Bulk modulus	1.59000E+08 (kPa)
Reference temperature	3.00000E+02 (K)	Reference temperature	3.00000E+02 (K)
Specific heat	4.77000E+00 (J/kgK)	Specific heat	4.77000E+00 (J/kgK)
Thermal conductivity	0.00000E+00 (J/mKs)	Thermal conductivity	0.00000E+00 (J/mKs)
Strength	**Elastic**	**Strength**	**von Mises**
Shear modulus	8.18000E+07 (kPa)	Shear modulus	8.18000E+07 (kPa)
Failure	**None**	Yield stress	8.00000E+05 (kPa)
Erosion	**None**	**Failure**	**None**
		Erosion	**None**

Load	$u_{AUTODYN}$ [mm]	u_{SDOF} [mm]
Blast	65.2	64.0
Fragment	11.0	13.9
Combined	85.7	139

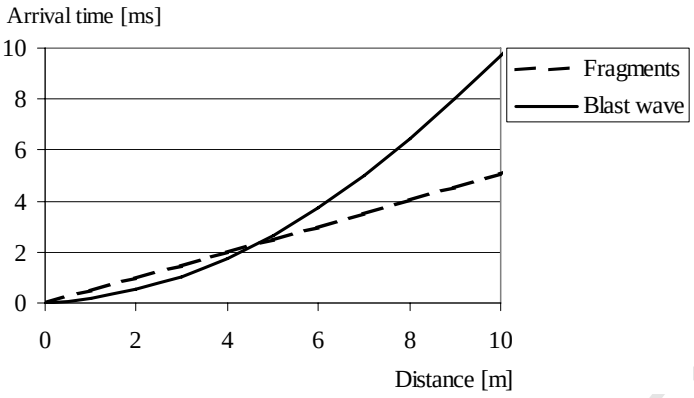

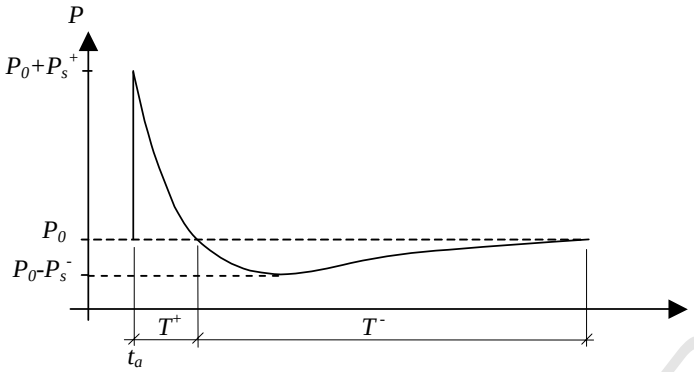

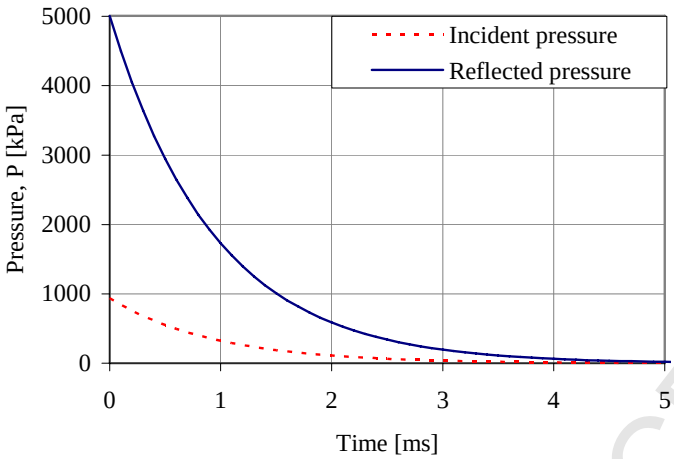

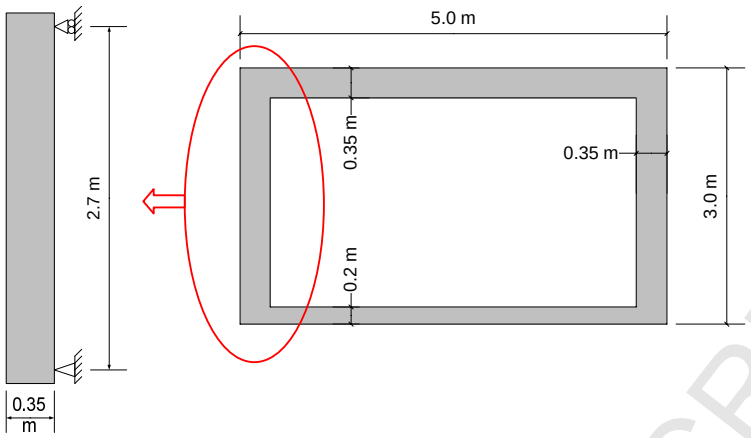

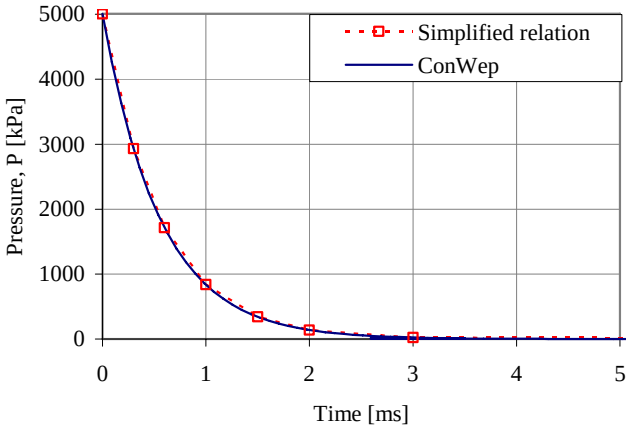

Time [ms]	Pressure [kPa]
0.0	5 006
0.3	2 930
0.6	1 713
1.0	836
1.5	340
2.0	137
3.0	22
8.974	0

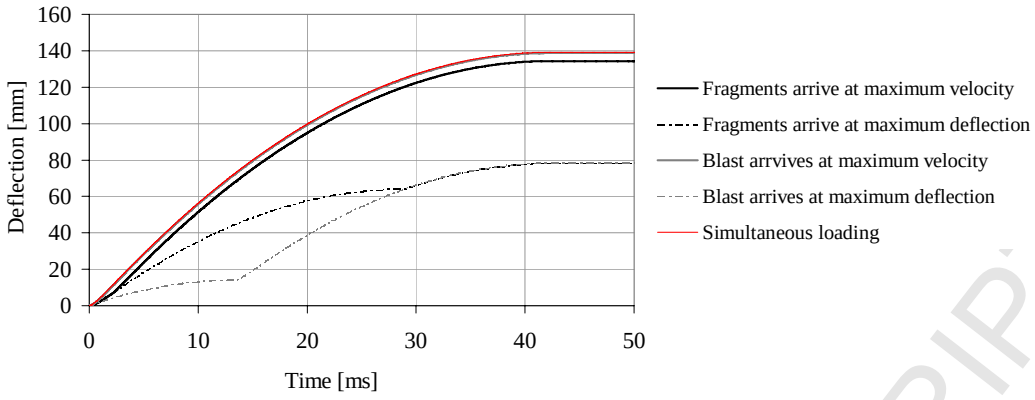

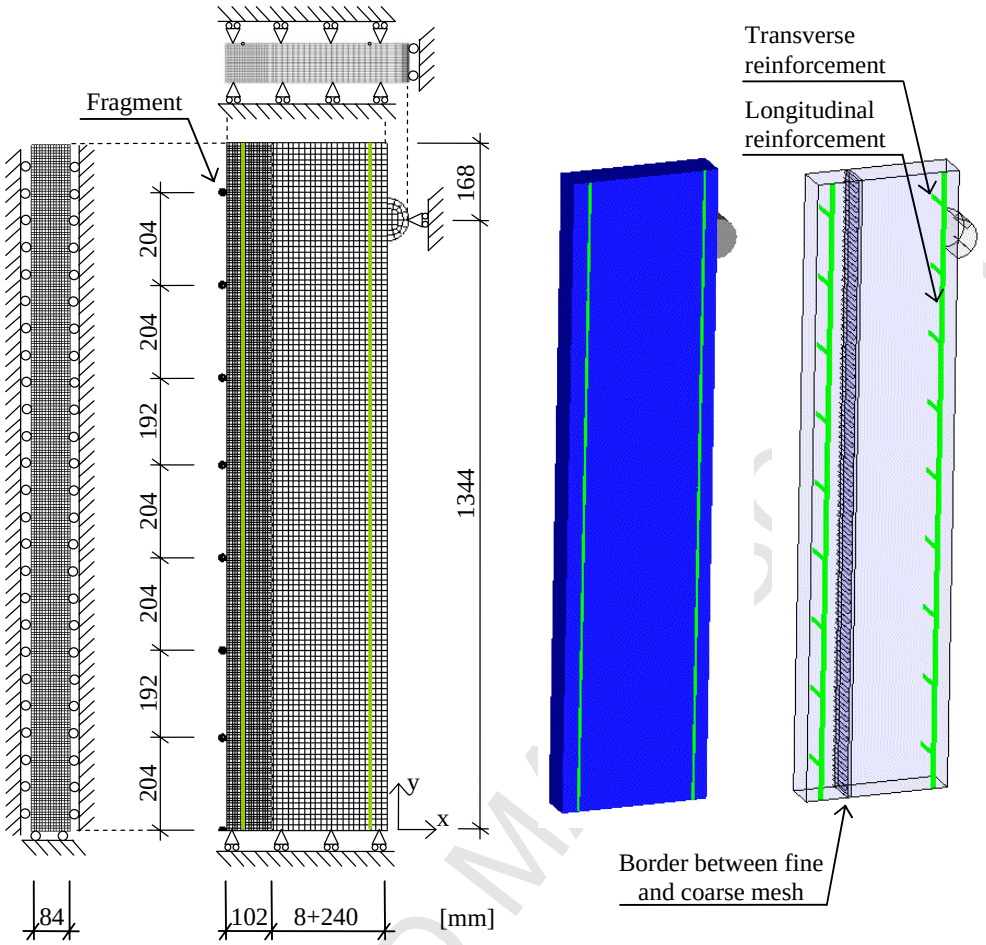

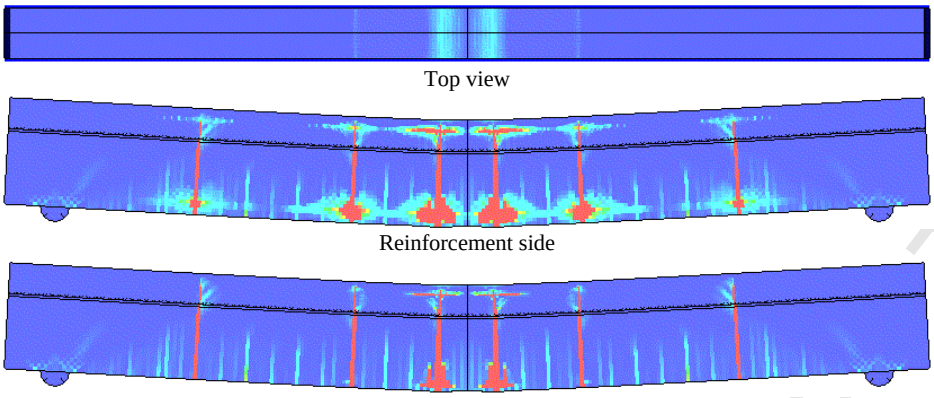

Top view

Reinforcement side

Middle of wall strip

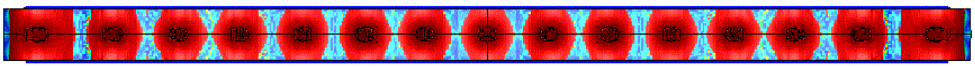

Top view

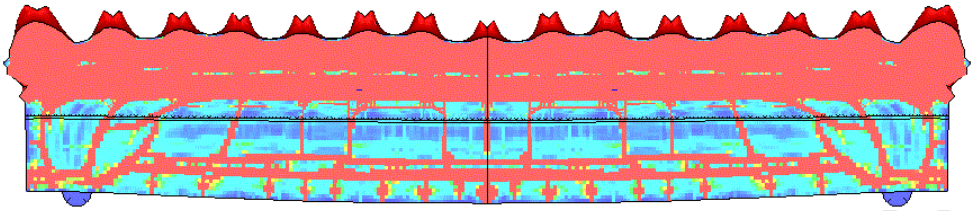

Reinforcement side

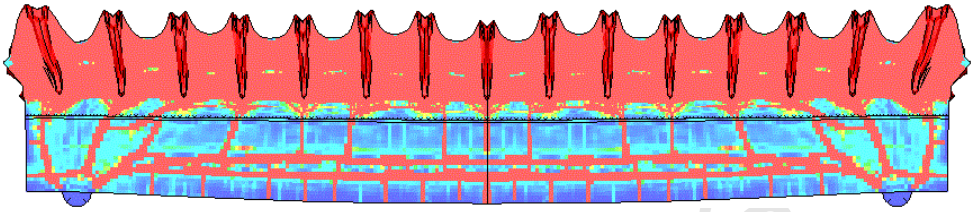

Middle of wall strip

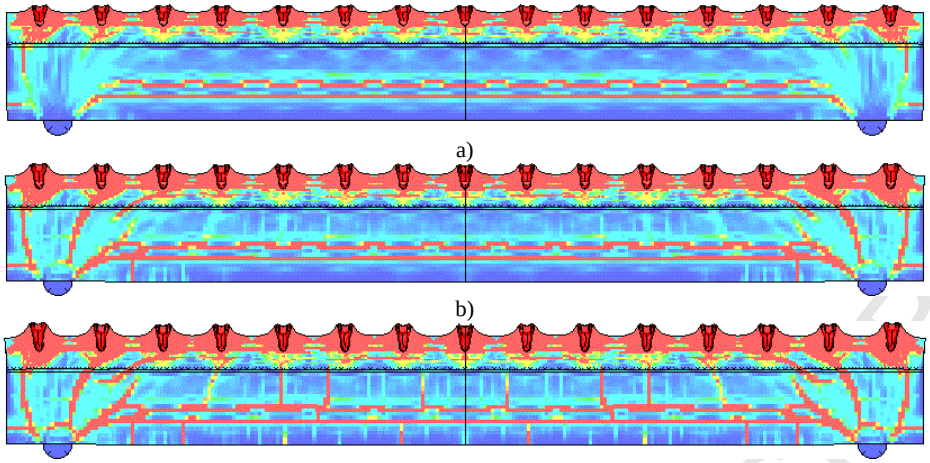

a)

b)

c)

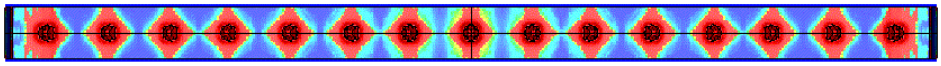

Top view

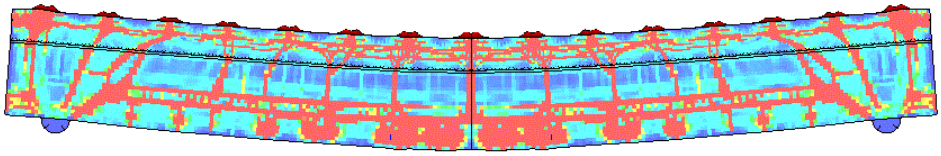

Reinforcement side

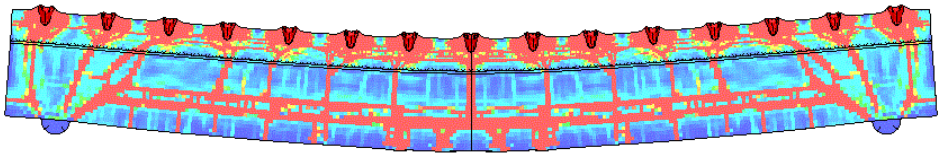

Middle of wall strip